# Intermediate-velocity atomic collisions. II. $K$-shell ionization and excitation in 8.6-MeV/amu Ca ions

Xiang-Yuan Xu,* E. C. Montenegro,† R. Anholt,‡ K. Danzmann, and W. E. Meyerhof
*Department of Physics, Stanford University, Stanford, California 94305*

A. S. Schlachter, B. S. Rude, and R. J. McDonald
*Accelerator and Fusion Research Division, Lawrence Berkeley Laboratory, University of California, Berkeley, California 94720*
(Received 28 December 1987)

Projectile $K$-shell ionization and excitation cross sections were measured for 8.6-MeV/amu $Ca^{19+,18+}$ beams incident on various gas targets. The ionization and excitation cross sections are compared with the Glauber approximation and with the plane-wave Born approximation. Various factors that may affect the ionization and the excitation cross sections in this intermediate-velocity regime, such as screening by the target electrons, polarization, and binding, are examined in order to establish their relative importance.

## I. INTRODUCTION

In recent years, our group has studied ionization and capture in ion-atom collisions in a regime in which the ratio $r_v$ of the relative velocity between the collision partners to the Bohr velocity of the active ($K$) electron is of the order of unity (intermediate-velocity regime). We varied the ratio $r_Z$ of the perturbing nuclear charge to the nuclear charge initially binding the active electron from values less than unity ("perturbative regime") to values greater than unity ("nonperturbative regime"). We did not find any sign of molecular effects, such as vacancy sharing between the collision partners, which are typical of slower collisions, i.e., with $r_v \lesssim 0.3$ and $r_Z \approx 1$.

It is a challenge to find suitable theories of ionization and electron capture which describe this intermediate-velocity regime for the whole range of $r_Z$. For ionization, we tried unsuccessfully to use the plane-wave Born approximation (PWBA), suitably modified by binding and polarization corrections introduced by Basbas *et al.*[1,2] for this velocity regime ($r_v \approx 1$), but limited to $r_Z \ll 1$. On the other hand, the Glauber approximation of McGuire *et al.*,[3,4] which stresses unitarity effects, reproduces the main trends of the ionization data. Similarly, for capture we found the Oppenheimer-Brinkmann-Kramers (OBK) approximation[5] unsuitable, but the nonrelativistic eikonal calculations of Eichler and Chan[6–8] reasonably successful. (Eikonal calculations stress the distortion of the captured electron wave function by the strongest nuclear potential in the collision.)

The present experiment examines ionization, and for the first time also excitation, in the intermediate-velocity regime with a projectile nuclear charge $Z_p = 20$. This fills a gap in the $Z_p$ values used by us to date ($Z_p = 6, 54, 92$).[9,10] As in our previous experiments, we measured ionization and excitation of projectile ($K$) electrons in order to avoid the disturbing effect of inner-shell vacancy formation by capture, as occurs in the study of target electron ionization by bare or few-electron projectiles. With the target atom acting as perturber, though, a complication arises due to screening effects which can either decrease the effective perturbation (potential screening) or increase it, due to ionization or excitation by individual target electrons (antiscreening). We have attempted to incorporate screening effects into the Glauber theory, using as basis a calculation of McGuire *et al.* for ionization of $H^0$.[3,4]

With the target atom acting as perturber on a projectile $K$ electron, the previously defined ratios $r_v$ and $r_Z$ are

$$r_v = v_p / v_{pK}, \quad r_Z = Z_t / Z_p , \tag{1}$$

where $v_p$ is the projectile velocity, $v_{pK}$ the Bohr velocity of a projectile $K$ electron, and $Z_t$ the target nuclear charge.

In this experiment 8.6-MeV/amu $Ca^{18+,19+}$ beams were used for which $r_v = 0.935$. The targets were gaseous and ranged from hydrogen to xenon, allowing the relative perturbing charges ($r_Z$) to vary from 0.05 to 2.7.

This paper is organized as follows. Section II describes the experimental methods for Ca projectile ionization and excitation measurements, as well as the data analysis. Section III presents the results obtained and makes comparisons with different theories for $K$-shell ionization. Finally, Sec. IV contains a summary of the main conclusions.

## II. EXPERIMENTAL METHOD AND DATA ANALYSIS

In this experiment, projectile ionization cross sections were obtained from the charge-state fractions observed after passage through the gaseous target. Excitation cross sections were determined from coincidence measurements between projectile $K$ x rays and the projectile charge-state fraction which had *not* undergone charge exchange in passage through the target.

Figure 1 displays the experimental apparatus used, which is based on an arrangement of Berkner *et al.*[11] A Ca-ion beam from the Lawrence Berkeley Laboratory Su-

 

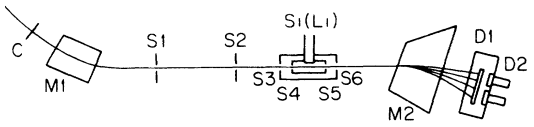


FIG. 1. Schematic diagram of the experimental apparatus. $C$, stripping foil; $M1$, charge selection magnet; $S1$,$S2$, upstream slits; $S3$–$S6$, gas-cell apertures; $M2$, magnetic spectrometer; $D1$, PPAC; $D2$, plastic scintillator counter system.

perHILAC was post-stripped in a carbon foil (C) to produce ions in high charge states, one of which was selected by the magnet $M1$. The resulting $Ca^{19+}$ or $Ca^{18+}$ beam was directed to the entrance of a differentially pumped gas cell ($S3$–$S6$) after having passed through a pair of collimating slits ($S1$ and $S2$). The beam emerging from the gas cell was charge analyzed by a second magnetic spectrometer $M2$ and directed into the detector box. X rays were detected by a 16-mm-diam Si(Li) detector placed into the gas cell at 90° with respect to the beam direction.

The diameters of the apertures $S3$–$S6$ were 2.0, 3.0, 3.9, and 3.9 mm, respectively, and the length of the gas cell (distance between $S4$ and $S5$) was 4.09 cm. Entrance and exit apertures $S3$ and $S6$ act as gas flow impedance, keeping the remaining beam line at about $10^{-6}$ Torr.

There were two kinds of detectors in the detector box, each of which could be moved separately into the beam. $D1$ was a position-sensitive parallel-plate avalanche counter (PPAC). $D2$ was a plastic scintillator counter system. The details of the PPAC construction and output is described in a previous paper.[9] We should mention, nevertheless, that the PPAC can be damaged when high count rates are used and thus it is not suitable for the coincidence measurements where high rates are required. In this case, the scintillator counter was used.

### A. Singles measurements

We used the PPAC to determine singles (noncoincident) charge-state distributions. For each target, the charge-state yields were measured at four or five target pressures and the relative counting rates were monitored in order to keep the system in the single-collision regime. For every projectile charge state, the yields with zero target pressure, which come mainly from the electron capture and loss in the residual gas in the beam line (except for the incident charge state), were measured at least four times.

The rate equations for the charge-state fractions $Y_n(x)$ at a thickness $x$ (in at./cm$^2$) are given by

$$\frac{dY_n}{dx}=\sum_{n'\neq n}[\sigma(n',n)Y_{n'}-\sigma(n,n')Y_n]\ , \tag{2}$$

where $\sigma(n',n)$ is the cross section for changing the $n'$ electrons attached to the projectile into $n$ electrons.

For thin targets, Eq. (2) can be approximated by

$$\begin{aligned} Y_{n_i}&\approx 1-\sum_{n\neq n_i}\sigma(n_i,n)x-O(x^2)\ ,\\ Y_n&\approx\sigma(n_i,n)x+O(x^2)\ , \end{aligned} \tag{3}$$

where $n_i$ is the number of electrons attached to the primary beam. Taking into account the yields $Y_{BG}$ measured in the absence of target gas, we can write

$$(Y_{n_i}-Y_{BG,n_i})/x\approx-\sum_{n\neq n_i}\sigma(n_i,n)+O(x)\ , \tag{4}$$

$$(Y_n-Y_{BG,n})/x\approx\sigma(n_i,n)+O(x)\ . \tag{5}$$

A term linear with $x$ on the right-hand side of Eqs. (4) and (5) would indicate a contribution due to double collisions. The left-hand side of Eqs. (4) and (5) is obtained experimentally. The quantity $x$ is proportional to the pressure inside the gas cell, which was measured using a calibrated capacitance manometer.[9] Using a least-squares fitting program, the cross sections $\sigma(n_i,n)$ can be obtained by extrapolating the left-hand side of Eq. (5) to the $x=0$ limit. Equation (4) serves as a check.

In the present experiment, the background yields $Y_{BG,n}$ ($n\neq n_i$) were always smaller than 0.1, and as a consequence $Y_{BG,n_i}$ was close to 1 for both the incident beams used. As the pressure in the gas cell was increased, the background also increased, but it was sufficiently flat under the charge-state peaks to be subtracted without serious errors. Because the gas purity was always better than 0.01%, the contribution from this source to the experimental uncertainties was small. In general, for the resulting ionization cross sections the uncertainties are approximately 10%.

### B. Coincidence measurements

As mentioned above, the scintillator counter system was used for coincidence measurements because the PPAC count rate had to be kept too low in this case. The plastic scintillator had a decay constant of its main component of about 2 nsec, and could be used to detect up to 10 000 particles/sec without serious damage. In the present experiment, the average count rate for every run was about 5000 sec$^{-1}$.

Two scintillators were used (named SR and SL). For each scintillator a 1-$\mu$m-thick Al foil was used to cover one-half of its sensitive area. The purpose of this procedure was to detect two adjacent charge states in one particle energy spectrum by taking advantage of the energy loss suffered by the particles directed to the covered region of the scintillator. In this way, when $Ca^{19+}$ was used as a projectile, $Ca^{19+}$ and $Ca^{20+}$ were recorded by SR and $Ca^{18+}$ and $Ca^{17+}$ were recorded by SL. The fast outputs of SR and SL were put in coincidence with the timing signal from the x-ray detector. The slow outputs of SR and SL were split, with one pulse going to a histogramming memory, the other into a computer ADC gated by a strobe signal. The block diagram of the electronics is displayed in Fig. 2.

The histogram data could be compared with the PPAC singles measurement. For SL, which did not accept the incident charge states, the difference between these two kinds of measurements was at most 20%. For SR, which accepted the incident projectile charge state (e.g., 19+), the ratio between $Ca^{20+}$ and $Ca^{19+}$ was higher than that one obtained with the PPAC. This discrepancy arose

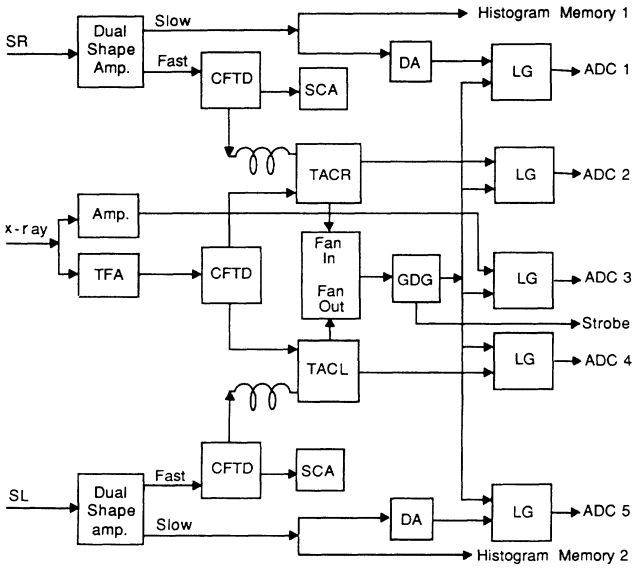


FIG. 2. Electronic block diagram for the coincidence measurement. CFTD, constant fraction discriminator; DA, delay amplifier; GDG, gate and delay generator; LG, linear gate; SCA, single channel analyzer; TAC, time-to-amplitude converter; TFA, timing filter amplifier.

from the pileup of the projectile (19+) signals which were the lower pulse-height signals in the detector. Consequently, we were not able to separate $Ca^{19+\to 19+}$ and $Ca^{19+\to 20+}$ (or $Ca^{18+\to 18+}$ and $Ca^{18+\to 19+}$) events in the coincidence measurements.

Ionization cross sections could be obtained absolutely from the charge-state measurements. Excitation cross sections (for $Ca^{19+}$), obtained from the coincidence measurements, were normalized to theoretical cross sections for $H_2$ and He targets (see Sec. III B).

We should note here one disadvantage of the foil (energy-loss) method. If the scintillator has been exposed to too high beam current, it is locally damaged and will cause pulses from a given charge state to appear in the wrong energy region. In the analysis of the coincidence measurements, we found some inconsistencies in the data which we attribute to this effect. Hence we assigned a ±30% uncertainty to the measured excitation cross sections.

## III. RESULTS AND DISCUSSION

### A. Ionization cross sections

The measured ionization cross sections of $Ca^{18+}$ and $Ca^{19+}$ projectiles are given in Table I. On the whole, the data for $Ca^{18+}$ are more precise than those for $Ca^{19+}$. Typical uncertainties for $Ca^{18+}$ are ±10%; the $Ca^{19+}$ uncertainties reach ±30%.

As discussed in Ref. 10, the single ionization cross section $\sigma_1(K^1)$ in $Ca^{19+}$ is found to be related to the single ionization $\sigma_1(K^2)$ in $Ca^{18+}$ by

$$\sigma_1(K^1)=\sigma_1(K^2)/2+\sigma_2(K^2)\ , \tag{6}$$

where $\sigma_2(K^2)$ is the double ionization cross section in $Ca^{18+}$. Due to the low statistics we were not able to determine any double ionization cross sections in the present experiment. From the data in Table I, it appears that within the experimental uncertainties, for all targets except $N_2$,

$$\sigma_1(K^1)\approx\sigma_1(K^2)/2\ . \tag{7}$$

Since the $Ca^{18+}$ data are more precise, we used Eq. (7) to compare the experimental one-electron ionization cross section with theory.

We analyzed the measured ionization cross sections by two distinct theories, the Glauber[3,4] and the PWBA (Refs. 1 and 2) approximations. The theoretical calculations, as well as the experimental data for the $Ca^{18+}$ beam, are shown in Fig. 3. In both approximations, the

TABLE I. Ionization cross sections ($10^{-20}$ cm$^2$/at).

| Target | $Ca^{18+}$ | $Ca^{19+}$ |
|---|---|---|
| $N_2$ | 12±2 | 3±1 |
| $O_2$ | 16±2 | 8±3 |
| Ne | 22±2 | 7±3 |
| Ar | 33±3 | 14±4 |
| Kr | 43±3 | 24±8 |
| Xe | 52±3 | 20±7 |

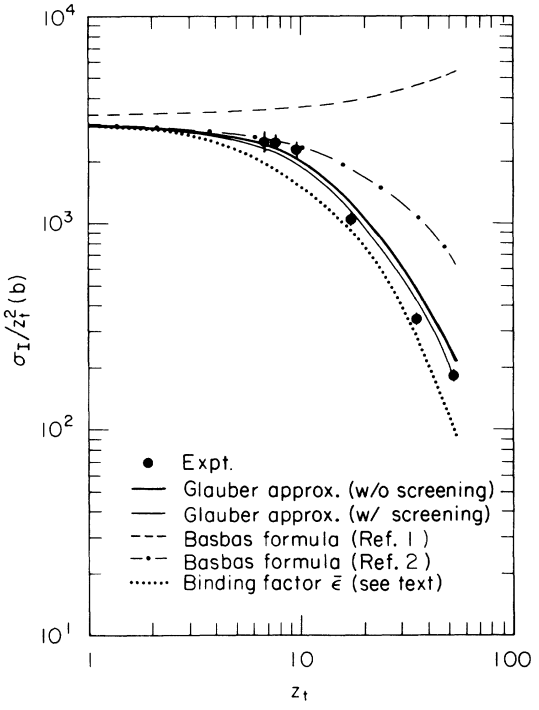


FIG. 3. Measured $Ca^{18+}$ ionization cross sections (●). The cross sections are divided by $Z_t^2$. The heavy curve is calculated using the Glauber approximation without screening and the light solid curve includes screening. The dashed curve is calculated from Ref. 1 and the dashed-dotted from Ref. 2. The dotted curve is the PWBA result using the binding factor $\bar{\epsilon}$, Eq. (10).

effective nuclear charge for the Ca $K$-shell electrons was set equal to 19.7.

Although the ratio between the perturbing charge $Z_t$ to that of the projectile can reach values approaching 3, it can be seen from Fig. 3 that the unscreened Glauber approximation[3,4] gives reasonable agreement with the experimental data. The cross sections in Fig. 3 were divided by $Z_t^2$ in order to eliminate the first-order perturbation theory dependence on $Z_t$. Despite this, there is a strong $Z_t$ dependence of the experimental data which is well followed by the Glauber calculations of Refs. 3 and 4.

An attempt to improve these Glauber calculations can be made by taking into account the target electron screening of the target nuclear charge. Recently, Salvat *et al.*[12] developed analytical Dirac-Hartree-Fock-Slater screening function for atoms. According to their work, the atomic form factor $F(q)$ can be written as

$$\frac{F(q)}{Z_t}=\sum_{i=1}^{3}\left[\frac{A_i\alpha_i^2}{\alpha_i^2+q^2}\right], \tag{8}$$

where $q$ is the momentum transfer and $A_i$ and $\alpha_i$ are tabulated constants. Including the screening of the target electrons, the Glauber ionization cross section can be written as[3,4]

$$\sigma_I=\sum_{l,m}\int dk\,dq\,|B(k,q,lm,1s)|^2\left[1-\frac{F(q)}{Z_t}\right]^2, \tag{9}$$

where $k$ and $lm$ are the momentum and the quantum numbers of the continuum final state, respectively, and $B$ is the unscreened Glauber ionization amplitude. Figure 3 displays (light solid line) the result of the calculation using Eq. (9), showing that a slightly better agreement with the experimental points is obtained, principally for the high-$Z$ targets.

As mentioned above, in the intermediate-velocity regime the ionization cross sections are quite sensitive to binding and polarization effects when the strength of the perturbing potential is increased. In contrast to the Glauber formalism, these effects can be easily included and separately analyzed by using the PWBA theory. Basbas *et al.*[1] developed a model to include these effects in target ionization. This model can also be applied to projectile ionization. Taking the cutoff constant between binding and polarization as in Ref. 7 ($c_K=1.5$), we obtained the dashed curve shown in Fig. 3. It is clear from the figure that this model is unable to reproduce the general behavior of the experimental data. The theory gives too large values for the cross sections (principally for large $Z_t$), which is an indication that the polarization effect is overestimated.

It is interesting to examine the behavior of the theoretical cross sections if the binding correction is included alone. The result of this approach using the formulas given in Ref. 2 (which corresponds to the limit $c_K\rightarrow\infty$) is shown by the dashed-dotted curve in Fig. 3. Although the general trend agrees with the experimental data, a large discrepancy remains in the high-$Z_t$ region. This behavior can be expected, since the Basbas theory is valid only in the $r_Z\ll 1$ regime.

Montenegro and Sigaud[13] used the adiabatic perturbation theory to study the ionization of the $1s\sigma$ molecular orbital in cases where the perturbing potential is not weak. An extention to nonadiabatic systems was done by imposing an asymptotic matching with the semiclassical approximation. The matching is achieved through an effective charge which connects the relaxation of the active and passive electrons to the evolution of the center of charge (in which the target wave functions are centered) during the collision process. This model can be applied to the systems considered here by noting that in the intermediate velocity regime the center of charge can be considered to lie at the projectile nucleus. Under these conditions, it is easy to show that the model of Ref. 13 is equivalent to the Basbas theory for projectile ionization with a modified binding factor (obtained through the parameter $\bar{\theta}$ of Ref. 13) given by

$$\bar{\epsilon}=\bar{\theta}/\theta=[1+Z_t g(\xi)/(Z_{pK}\theta)]^2, \tag{10}$$

where $\theta=I/Z_{pK}^2$, $I$ is the projectile $K$-shell ionization energy and $\xi=2v_p/\theta Z_{pK}$. It should be noted that if $Z_t\ll Z_{pK}$ ($r_Z\ll 1$), Eq. (10) gives $\bar{\epsilon}\approx\epsilon\approx 1+2Z_t g(\xi)/\theta Z_{pK}$ which is the Basbas factor for projectile ionization.

The dotted curve in Fig. 3 shows the result of the calculations using the PWBA with the binding factor given by Eq. (10). The improvement for high-$Z$ targets is significant, compared with the Basbas factor. It is reasonable, also, that a calculation which includes only the binding factor should lie below the experimental points in order to allow for the manifestation of the polarization effect.

### B. Excitation cross sections

The measured excitation cross sections for $Ca^{19+}$ and $Ca^{18+}$ projectiles are given in Table II. The comparison between these two data sets requires a more careful analysis than the simple statistical considerations used in Eq. (6). First, the heliumlike $Ca^{18+}$ ions may be excited to metastable states which do not decay within the view of the detector. A detailed analysis including these states shows that nevertheless the same x-ray production cross section should be expected for $Ca^{18+}$ and $Ca^{19+}$ beams.[14] Second, second-order processes such as two-electron excitation, ionization followed by electron capture into the projectile $L$ or higher shells or simultaneous excitation and ionization (the $Ca^{18+}$ beam was not separated from

TABLE II. Excitation cross sections ($10^{-20}$ cm$^2$/at). (All cross sections are normalized to the PWBA theory at $Z_t=1$ and 2 and have a relative uncertainty of ±30%.)

| Target | $Ca^{18+}$ | $Ca^{19+}$ |
|---|---|---|
| $H_2$ | 0.3 | 0.15 |
| He | 0.9 | 0.4 |
| $N_2$ | 9 | 5 |
| $O_2$ | 10 | 6 |
| Ne | 13 | 10 |
| Ar | 19 | 11 |
| Kr | 32 | 20 |
| Xe | | 24 |

the $Ca^{19+}$ beam, as mentioned previously) prevent a clear interpretation of the $Ca^{18+}$ data. Although the two-electron processes can explain qualitatively the increase of the $Ca^{18+}$ cross section compared to the $Ca^{19+}$ one, it is a complex task to obtain any quantitative estimate for these processes. Hence we restrict this paper to the analysis of the $Ca^{19+}$ excitation.

The $K$ x-ray production cross section is assumed to be given by

$$\sigma_x = \left[\sum_n \sigma_{1s-n}\right] - \sigma_{1s-2s} , \tag{11}$$

where $\sigma_{1s-n}$ is the excitation cross section from the $1s$ state of $Ca^{19+}$ to the bound state $n$. In the PWBA, $\sigma_{1s-n}$ and $\sigma_{1s-2s}$ are given by[5]

$$\sigma_{1s-n} = \sigma_0 \int_{q_{\min}}^{\infty} dq \frac{2^9}{3n^3}(3q^2+1-n^{-2})[(q^2+(1-n^{-1})^2]^{n-3}/\{q[q^2+(1+n^{-1})^2]^{n+3}\} , \tag{12}$$

$$\sigma_{1s-2s} = \sigma_0 \int_{q_{\min}}^{\infty} dq \frac{2^6 q}{(q^2+\frac{9}{4})^6} , \tag{13}$$

$\sigma_0 = 4\pi(Z_t/v_p)^2$, and $q_{\min} = (1-n^{-2})Z_p/2v_p^2$. Atomic units are used in the above equations. The cross section $\sigma_{1s-2s}$ was removed from the total x-ray production cross section because the $2s$ metastable state of hydrogen-like $Ca^{19+}$ does not decay within the view of the detector. Other states with higher $n$ that can eventually cascade into the $2s$ state give a very small contribution to the total cross section and can be neglected. In Eq. (11), the sum over $n$ was carried up to $n=7$.

Figure 4 shows the scaled experimental x-ray excitation cross sections $\sigma_{ex}$ as a function of $Z_t$ and compare them with Glauber and PWBA results. The experimental cross sections are normalized at $Z_t=1$ and 2 to the PWBA theory. Glauber calculations were based on the $1s$-$2p$ excitation cross section of Franco and Thomas.[15] PWBA cross sections were obtained directly from Eqs. (11)–(13) (dashed line) and by changing the minimum momentum transfer in these equations in order to include a binding factor (dotted line). The binding factor for the excitation can be taken approximately as the same for the ionization (it can be shown that within the semiclassical approximation, the shape of impact parameter dependence of the ionization probability is the same for any $s$-$s$ transition[16]) and the new minimum momentum transfer becomes

$$\bar{q}_{\min} = \bar{\epsilon} q_{\min} , \tag{14}$$

with $\bar{\epsilon}$ given by Eq. (10).

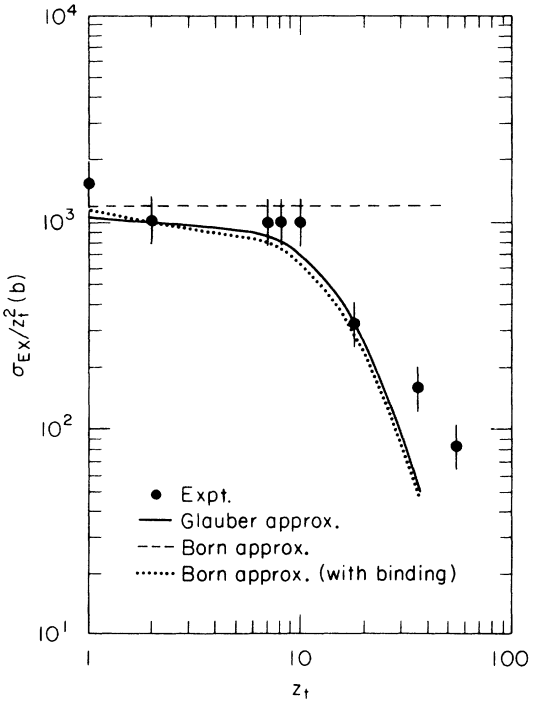


FIG. 4. Measured $Ca^{19+}$ excitation cross sections (●). The cross sections are divided by $Z_t^2$. The solid curve is the Glauber approximation. The dashed line is the result given by the Born approximation and the dotted one is the Born approximation with the binding effect included [Eqs. (11)–(14)].

Glauber and PWBA (with binding) results have almost the same behavior, both following the general trend of the experimental data. Despite the relatively large experimental error, there appears to be a significant deviation for the higher-$Z$ targets. This discrepancy can be a consequence of the contribution from simultaneous ionization and capture. In such a process, the $Ca^{19+}$ electron is ejected while another electron from the target atom is captured into the $L$ or higher shell. In the present case the capture cross section always increases with $Z_t$ because more electrons with velocity near $v_p$ are available to be captured.[14] Since the ionization cross section also increase with $Z_t$ (see Table I), this two-electron process is likely to contribute to the increase of the x-ray production cross sections compared to the first-order excitation mechanism.

## IV. CONCLUSIONS

Because electron capture has a strong dependence on the charge state of the incident ion, the study of the target ionization by strongly perturbing potentials is, in many cases, frustrated by a substantial contribution due to the capture channel. In these cases, projectile ionization is particularly appropriate since it avoids not only the electron capture contribution but also other complications such as the change of fluorescence yields due to

the multiple ionization of the target.

The measurements of projectile ionization presented in this paper demonstrate the effect of the increasing strength of the perturbing potential in the intermediate velocity region ($v_p \sim v_{pK}$). Within the PWBA, a main conclusion is that the polarization of the active electron wave function is a small effect that does not greatly influence the strong reduction of the cross section due to the binding effect. In this sense, the prescription given by Basbas *et al.*[1] is not supported by this experiment.

Both the Glauber theory and the PWBA with the modified binding factor alone given by Eq. (10), give a reasonable description of the ionization and excitation data. As a matter of fact, it is intriguing that these two theories give very similar results. As pointed out by Anholt *et al.*,[17] it is not clear how the physical ideas behind the Glauber approximation and the binding effect in the PWBA can be compared. It is possible that an examination of unitarity which is included in the Glauber approximation, but not in the PWBA, will help to clarify this point. Finally, it should be noted that the general agreement between the present PWBA calculations and experiment indicates that the scaling laws which emerge from PWBA based low velocity theories[2,13] can be extended to the intermediate velocity regime and for a large range of collision symmetries. Naturally, in the latter case, the binding correction should include the higher-order contributions from the perturbing charge as suggested by Eq. (10).

## ACKNOWLEDGMENTS

We thank J. W. Stearns for his help in the data acquisition. This work was supported in part by the National Science Foundation under Grant No. 86-14650 and by the U. S. Department of Energy, Division of Chemical Sciences, Office of Fusion Energy, under Contract No. DE-AC03-76SF00098. One of us (E.C.M.) acknowledges support from Conselho Nacional de Desenvolvimento Cientifico e Tecnológico (Rio de Janeiro, Brazil).

---

*Permanent address: Department of Physics, Tsinghua University, Beijing, People's Republic of China.

†On leave from Pontificia Universidade Catolica, do Rio de Janeiro, Brazil.

‡Present address: Solid State Electronics Laboratory, Stanford University, Stanford, California.

[1]G. Basbas, W. Brandt, and R. Laubert, Phys. Rev. A **17**, 1655 (1978).

[2]G. Basbas, W. Brandt, and R. Laubert, Phys. Rev. A **7**, 983 (1973).

[3]J. E. Golden and J. H. McGuire, Phys. Rev. A **12**, 82 (1975).

[4]J. H. McGuire, Phys. Rev. A **16**, 143 (1982).

[5]M. R. C. McDowell and J. P. Coleman, *Introduction to the Theory of Ion-Atom Collisions* (North-Holland, Amsterdam, 1970).

[6]J. Eichler and F. T. Chan, Phys. Rev. A **20**, 104 (1979).

[7]F. T. Chan and J. Eichler, Phys. Rev. A **20**, 184 (1979).

[8]J. Eichler, Phys. Rev. A **23**, 498 (1981).

[9]R. Anholt, X.-Y. Xu, Ch. Stoller, J. D. Molitoris, W. E. Meyerhof, B. S. Rude, and R. J. McDonald, paper I, Phys. Rev. A **37**, 1105 (1988).

[10]R. Anholt, W. E. Meyerhof, X-Y. Xu, H. Gould, B. Feinberg, R. J. McDonald, H. E. Wegner, and P. Thieberger, Phys. Rev. A **36**, 1586 (1987). Earlier references are given in this paper.

[11]K. H. Berkner, W. G. Graham, R. V. Pyle, A. S. Schlachter, and J. W. Stearns, Phys. Rev. A **23**, 2891 (1981).

[12]F. Salvat, J. D. Martinex, R. Mayal, and J. Parellada, Phys. Rev. A **36**, 467 (1987).

[13]E. C. Montenegro and G. M. Sigaud, J. Phys. B **18**, 299 (1985).

[14]E. C. Montenegro, X.-Y. Xu, W. E. Meyerhof, R. Anholt, K. Danzmann, A. S. Schlachter, B. Rude, and R. J. McDonald, following paper, Phys. Rev. A **38**, 1854 (1988).

[15]V. Franco and B. K. Thomas, Phys. Rev. A **14**, 945 (1971).

[16]E. C. Montenegro and A. G. de Pinho, J. Phys. B **15**, 1521 (1982); **15**, L565 (1982).

[17]R. Anholt, W. E. Meyerhof, H. Gould, Ch. Munger, J. Alonso, P. Thieberger, and H. E. Wegner, Phys. Rev. A **32**, 3302 (1985).